

Ultra-broadband co-polarization anomalous reflection metasurface

Jingfan Yang¹ · Shaobo Qu¹ · Hua Ma¹ · Jiafu Wang¹ · Sai Sui¹ · Qiqi Zheng¹ · Hongya Chen¹ · Yongqiang Pang¹

Received: 29 December 2016 / Accepted: 19 July 2017 / Published online: 24 July 2017
© Springer-Verlag GmbH Germany 2017

Abstract In this paper, an ultra-broadband co-polarization anomalous reflection metasurface was proposed. The metasurface was constructed by two crossed H-shaped metallic pattern, which can be seen as electric dipole resonator. Whether the incident waves were left-handed circularly polarized (LCP) or right-handed circularly polarized (RCP), the co-polarization reflective efficiency was more than 97% over ultra-broadband from 8.17 to 19.3 GHz. It was noticeable that the ultra-broad band was achieved through the superposition of multiple resonance bands. By decomposing the circular polarization (CP) waves into two linear polarization (LP) waves, one of which was *x*-direction LP wave and the other was *y*-direction LP wave, the reflective matrix was used to explain the mechanism of high efficient co-polarization reflection. By utilizing the proposed co-polarization reflection unit cell, a kind of phase gradient metasurface was achieved based on Pancharatnam–Berry Phase (PB phase). At last, simulation results and measurement results showed a good accordance, indicating that the proposed metasurface did have great co-polarization anomalous reflection effects.

1 Introduction

As is known to us all, metasurfaces were considered as a kind of quasi two-dimensional artificial metamaterials, which featured in sub-wavelength thickness, periodic arrays and inhomogeneous unit cells. Traditionally, the

research on metasurfaces mainly focused on the electromagnetic wave frequency selectivity, which usually confined the concept of metasurfaces to frequency selective surface (FSS) and ignored other properties. In fact, nearly all fundamental properties of EM waves can be tailored by metasurface, such as phase, polarization state, amplitude, and so on [1–12]. As for light frequency, wave propagation path was tailored by optical elements and diffractive structures (gratings) through gradual phase accumulation [13–15], while as for microwave frequency, conventional methods would enlarge the size of elements, restricting the components application. However, sub-wavelength resonators can achieve abrupt phase change, in this case, through artificially arranging these resonate arrays, abrupt phase changes can be achieved. And the artificial resonator arrays are named phase gradient metasurface (PGMs). That is to say, through elaborately designing the gradient of PGMs, the reflective/refractive waves propagation path could be controlled as desired [16, 17]. A broadband anomalous reflection metasurface under specific polarization statement was achieved by H-shaped structure array [18]. Anomalous refraction was demonstrated by spatially assembly of short metallic nanowires with different rotation degrees under the circular polarization illumination [19]. Traditional polarization manipulation was mainly relied on multilayered metallic structures which led to bulky thickness and narrow working spectrum [20]. In this view, metasurfaces hold incomparable advantages. Light polarization manipulation was demonstrated by orthogonal elongated nano-rods and complementary nano-slits arrays [21]. A broadband optical circular polarization converter was demonstrated by gold helix structures [22]. The terahertz-wave polarization rotator was demonstrated by S-shape resonators [23]. In general, compared to linear-to-linear polarization and linear-to-circular polarization

✉ Yongqiang Pang
225pang@163.com

¹ College of Science, Air Force Engineering University, Xi'an 710051, People's Republic of China

conversion, there were fewer studies on circular polarization. Usually, when a circular polarization wave incident on conventional interface, the reflective wave always changes into cross-polarization [24]. For example, if the incident wave is a left-handed circular polarization, the reflective wave will change into right-handed circular polarization.

Here, a kind of metasurface which combined ultra-broadband circular polarization-keeping reflection with anomalous reflection was proposed. This metasurface is constructed by two crossed H-shaped metallic array which is backed with a metal background. Due to the anisotropy of this structure, no matter what polarization the incident waves are, the co-polarization of reflective waves efficiency can be larger than 90% during the wideband from 7.8 to 20 GHz. Then through arraying spatially six units with different rotation angle, a kind of metasurface with ultra-broadband circular polarization-keeping and anomalous reflection has been achieved. Experimental results show a great consistency with simulated results.

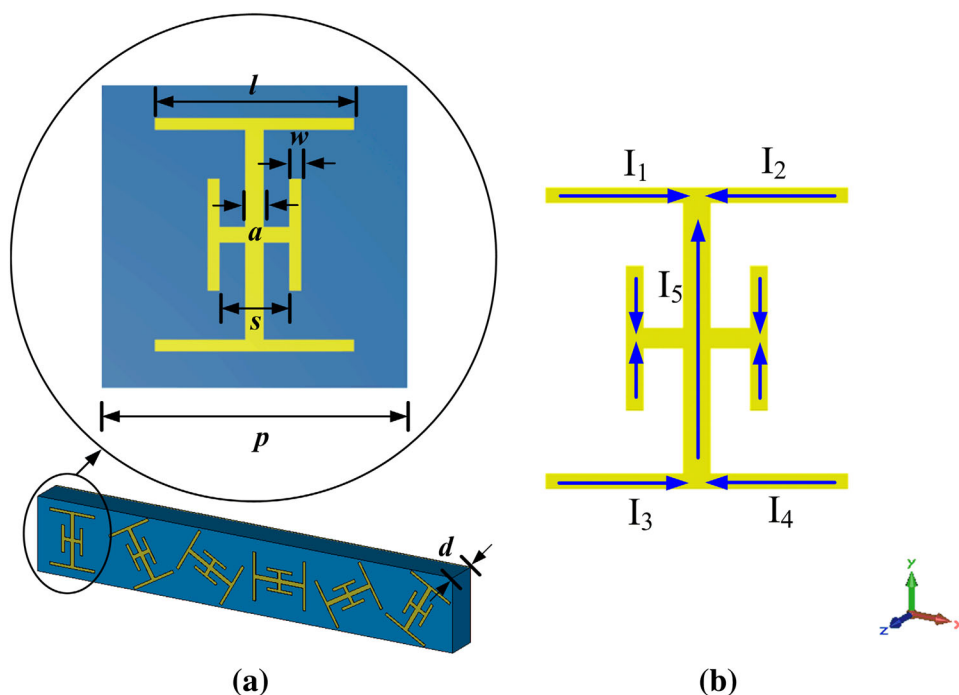
2 Design of metasurfaces

As is shown in Fig. 1a, it shows the schematic picture of the metasurface. From the schematic, we can see that the unit cell is constructed of two crossed H-shaped metallic pattern with a metallic background. And the top metallic pattern and bottom metallic ground sheet was spaced by dielectric layer. The metallic ground sheet served as

reflection mirror, which blocks the incident wave transmission and helps the proposed metasurface reflects the entire incident wave. And the high efficiency of circular polarization-keeping reflection stems from the resonances which were stimulated by the resonator composed by upper metallic pattern and the metallic background. The ultra-broadband working bandwidth was owing to the superposition of four resonances. To get the perfect effects, all the parameters designed in the unit cell is optimized through parameters sweep, and the optimized dimensional parameters were determined as: $p = 6.6$, $l = 4.29$, $s = 1.51$, $w = 0.25$, $a = 0.39$, $d = 3$. And corresponding dielectric was chosen as the specific parameters ($\epsilon = 2.65$ and $\tan\delta = 0.001$).

To further explain the detailed mechanism of circular polarization-keeping reflection, we take the LCP wave incidence for example, and decompose the incident LCP waves into two linearly polarized (LP) incident waves. Hence, corresponding electric field vector E_i of the incident waves can be also decomposed into two parts, which are perpendicular to the incidence. Taking a specific point in the field for example, the electric field parts can be supposed as E_{ix} and E_{iy} . Given the situation that the incident waves is LCP waves, the corresponding resonance occurs in the two crossed H-shaped metallic pattern. As is shown in the Fig. 1b, the surface induced current was described as the blue arrowed lines. Because the symmetric of the metallic pattern, we supposed that $I_1 = I_2$, $I_3 = I_4$. And from the view of x direction, the entire current can be considered as counter-balance. Consequently, the whole

Fig. 1 **a** Graphic of metasurface, the upper schematic shows the *front view* and the *bottom schematic* gives the perspective view. **b** The schematic of *top* metallic pattern and its surface current direction under vertical polarization the LCP waves incidence



surface currents were concentrated in the y -direction. The two crossed H-shaped metallic pattern can be seen as a dipole in y -direction. And it effected the phases of the reflected field of the reflection waves. The phases shifts in x and y -direction caused by electric dipole results in the polarization conversion. That is to say, when illuminated by LCP waves, the polarization-keeping of the reflective waves has achieved due to the reversed polarization and propagation. So it is with RCP waves. The two crossed H-shaped metallic pattern and metal background can be seen as Fabry–Perot resonator, so the high efficiency of co-polarization reflection is accomplished by multi-reflection. As for the anomalous reflection under circular polarization wave incidence, according to the principle of phase gradient metasurface, phase shift of reflected waves could be obtained by different two crossed H-shaped metallic pattern with rotated angle.

3 Simulations and analysis

To validate our previous design, CST microwave Studio, numerical simulations were carried out for this PGM in 5–25 GHz. First, we take the single unit cell for simulation. The boundary conditions were set as unit cell boundary, and the incidence was circular polarization waves. The corresponding simulated co-polarized and cross-polarized reflection efficiency results were given in Fig. 2, where r_{LR} (r_{RL}) denotes the amplitude of cross-polarized reflected waves under LCP (RCP) waves incident and r_{LL} (r_{RR}) stands for amplitude of co-polarized reflected waves under LCP (RCP) waves incident.

It is obviously to see from the Fig. 2 that during a broad frequency band from 8.17 to 19.3 GHz, the efficiency of

the co-polarization reflection was over 97%, and the cross-polarized part was less than 3%. The simulation results exhibit an ultra-broadband and highly efficiency CP-keeping reflection metasurface. The ultra-broadband reflection results is due to the superposition of multiple co-polarization keeping frequency peaks at 8.63, 12.23, 18.07 and 22.16 GHz which is corresponding to the four resonance frequencies. However, the 22.16 GHz frequency peak was too far away from its nearest frequency peak, it did not form a very high efficient performance. The highly efficiency working frequency band has defined to 8.17 to 19.3 GHz.

To analyze the polarization more detailedly, field monitor was used to track the simulated surface current distribution on the two crossed H-shaped metallic pattern. Figs. 3 and 4 stand for LCP and RCP incident waves, respectively. While 3a and 4a, 3b and 4b, and 3c and 4c stand for $f = 8.63$ GHz, $f = 12.23$ GHz, and $f = 18.07$ GHz. As can be seen from the schematic, the calculated surface current accords well with the previous analysis in Fig. 1b.

From above surface current distribution we can see that, the surface currents were uneven. When responding to electric field of incident field, the resonance between surface current and incident electric field may produce phase changes in reflective waves and transmitted waves. We suppose that when the incidence wave is LCP, the reflected electric field is denoted as E_{rx} and E_{ry} , respectively, and can be defined as

$$E_{rx} = \hat{x}r_x E e^{i\phi_x}, \quad E_{ry} = \hat{y}r_y E e^{i(\phi_y + \pi/2)} \tag{1}$$

The incident CP waves can be decomposed into two LP waves, one is x -polarized and y -polarized one. Learned from LP waves reflection matrix:

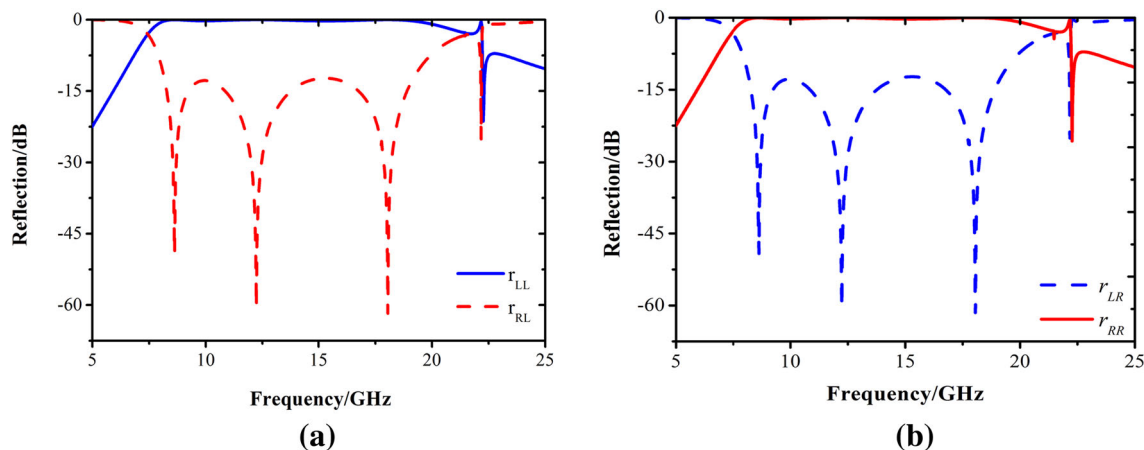


Fig. 2 Calculation results of co-polarized and cross-polarized efficiency under CP waves. **a** Co- and cross-polarized reflected waves under *left*-handed polarization incidence. **b** Co- and cross-polarized reflected waves under *right*-handed polarization incidence

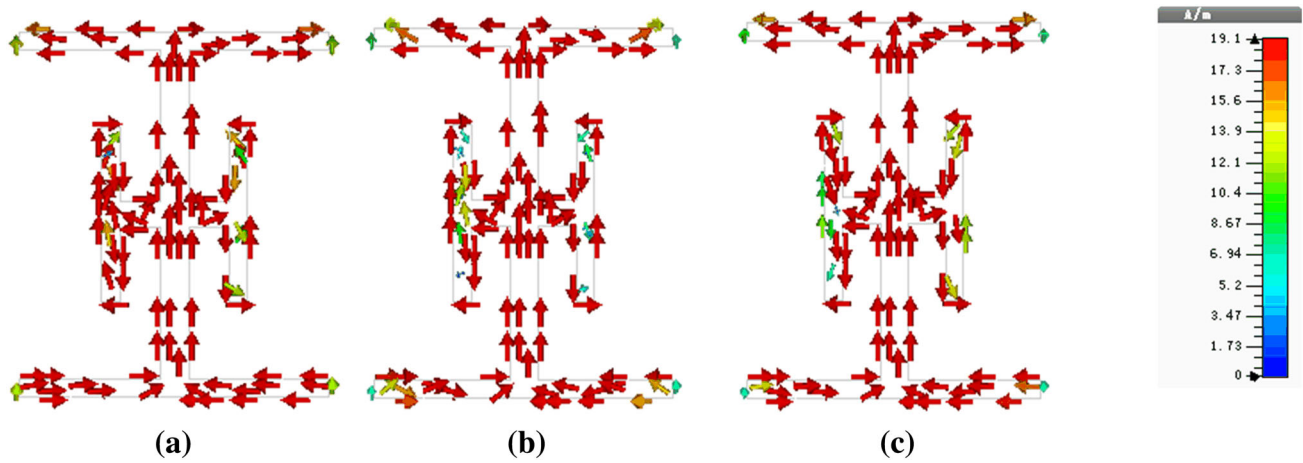


Fig. 3 Calculated surface current values of magnitude under LCP polarization, **a** $f = 8.63$ GHz, **b** $f = 12.23$ GHz, **c** $f = 18.07$ GHz

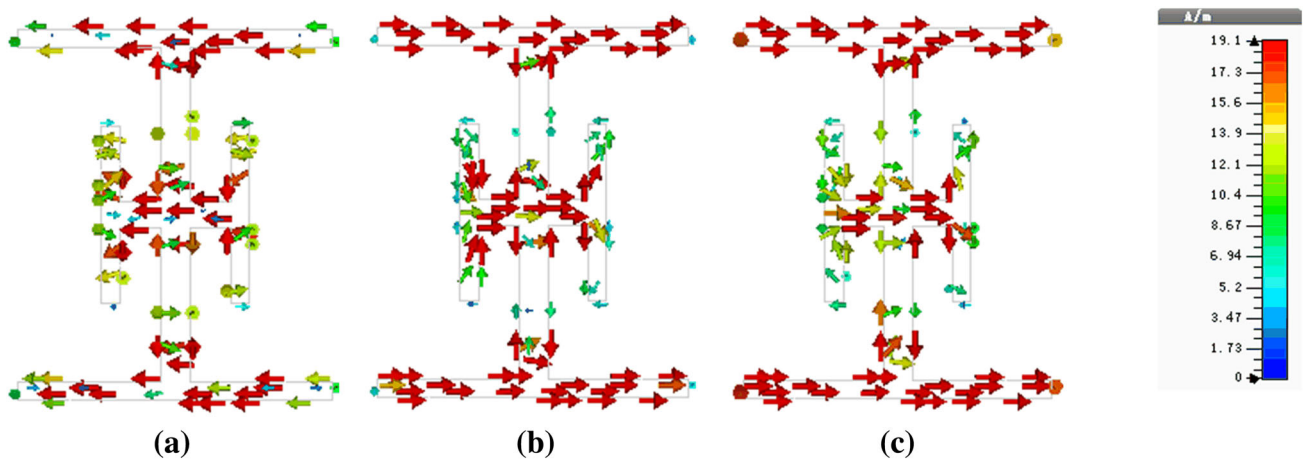


Fig. 4 Calculated surface current values of magnitude under RCP polarization, **a** $f = 8.63$ GHz, **b** $f = 12.23$ GHz, **c** $f = 18.07$ GHz

$$\begin{pmatrix} E_{Rx} \\ E_{Ry} \end{pmatrix} = \begin{pmatrix} R_{xx}e^{i\phi_{xx}} & R_{xy}e^{i\phi_{xy}} \\ R_{yx}e^{i\phi_{yx}} & R_{yy}e^{i\phi_{yy}} \end{pmatrix} \begin{pmatrix} E_{ix} \\ E_{iy} \end{pmatrix} \quad (2)$$

So, the reflected electric field was calculated as

$$E_R = (R_{xx}E_{ix}e^{i\phi_{xx}} + R_{xy}E_{iy}e^{i\phi_{xy}})\hat{x} + (R_{yx}E_{ix}e^{i\phi_{yx}} + R_{yy}E_{iy}e^{i\phi_{yy}})\hat{y}. \quad (3)$$

The LP reflection waves amplitude were composed of R_{xy} , R_{xx} , R_{yx} , R_{yy} , where the subscript of R means the incident waves polarization state and the reflective waves polarization state. Taking R_{xy} for example, it means the x -polarized reflective waves amplitude under the y -polarized incidence.

And CP waves can be decomposed into two LP waves, so there exists 90° phase delay relationship in x and y -direction of electric field. When reflected, a π phase shift takes place in x and y -direction. Since the propagation direction is reversed when the CP wave is incident on the surface, there must be an inverse phase delay between the x and y -directions if the co-polarization is achieved, i.e., $\phi_{yy} - \phi_{xx} = \pm\pi$.

Meanwhile, we also take the phase differences of co-polarized and cross-polarized reflective waves under LCP incident into consideration. Shown in Fig. 5. It is obviously to notice that where there exists π -phase jump, which just verified our analysis. We can see that the phase shift value is more than π at 22.16 GHz, which accorded with our previous explanation about the fourth resonance peak.

4 Phase gradient metasurface analysis

In traditional PGMs design, the resonance frequency was associated with the size of the unit cell and every size has a corresponding resonance frequency. So the abrupt phase change of the reflective wave varies with the size of the unit cell. Through the superposition of different size of unit cell, we can widen the working bandwidth. In this work, based on PB phase, we used six co-polarization reflection unit cell with different rotation angle to form this PGMs. According to the PB phase theory, different reflection

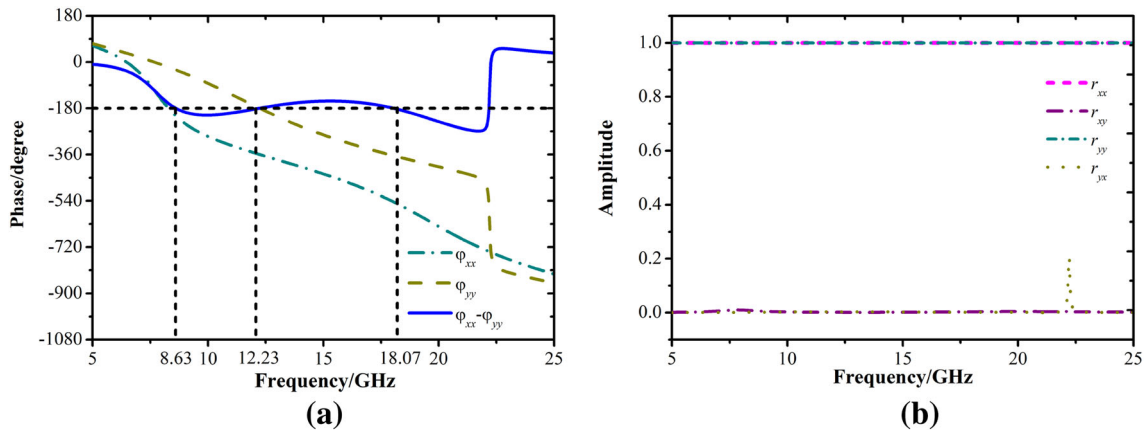


Fig. 5 **a** Phase differences of co-polarized under LP incidence. **b** Reflection efficiency of co-polarized reflected waves

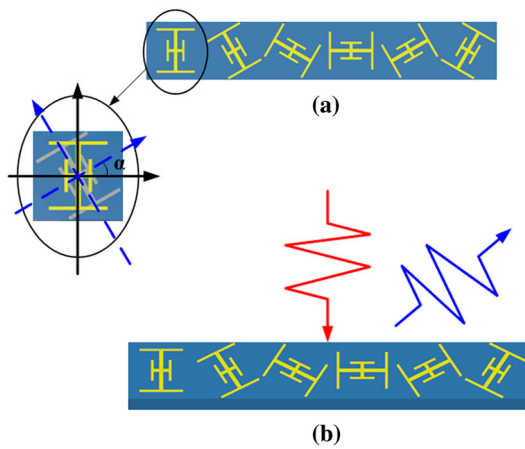


Fig. 6 **a** Schematic of reflective PGM. **b** Expected effects of PGM

phase shifts occur under CP polarization when the unit cell of metasurface rotates for a specific angle. It has been proven that the reflection phase difference $\Delta\phi$ and unit cell rotated angle α were related:

$$\Delta\phi = \pm 2\alpha \tag{6}$$

where ‘+’ means that the incidence wave is LCP and ‘-’ means RCP wave incidence. Correspondingly, the phase gradient is calculated as

$$\nabla\phi = \frac{\Delta\phi}{p} \tag{7}$$

where p is the periodic of the resonator array.

Given a situation that CP waves are incident onto the PGMs with an random incident angle θ_i , and based on the generalized Snell law [25], the anomalous reflected angle was calculated by [25]

$$\theta_r = \arcsin\left(\frac{k_0 \sin\theta_i + \nabla\phi}{k_0}\right) \tag{8}$$

where k_0 is the free space wave-vector.

In our work, we desired to obtain $\Delta\phi = \pi/3$ phase shift, so according to the formulation, we set the rotated angle $\alpha = 30^\circ$. The detail schematic view of the metasurface was displayed in Fig. 6a.

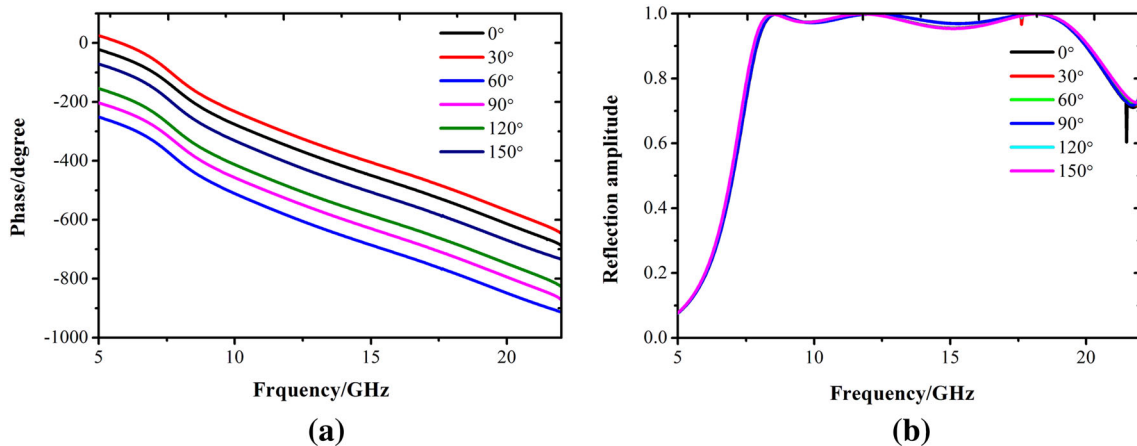


Fig. 7 The simulation of amplitudes and phases of co-polarized reflected waves of each unit cell with different rotation angle under LCP waves incidence. **a** The phases shift **b** the reflection amplitude

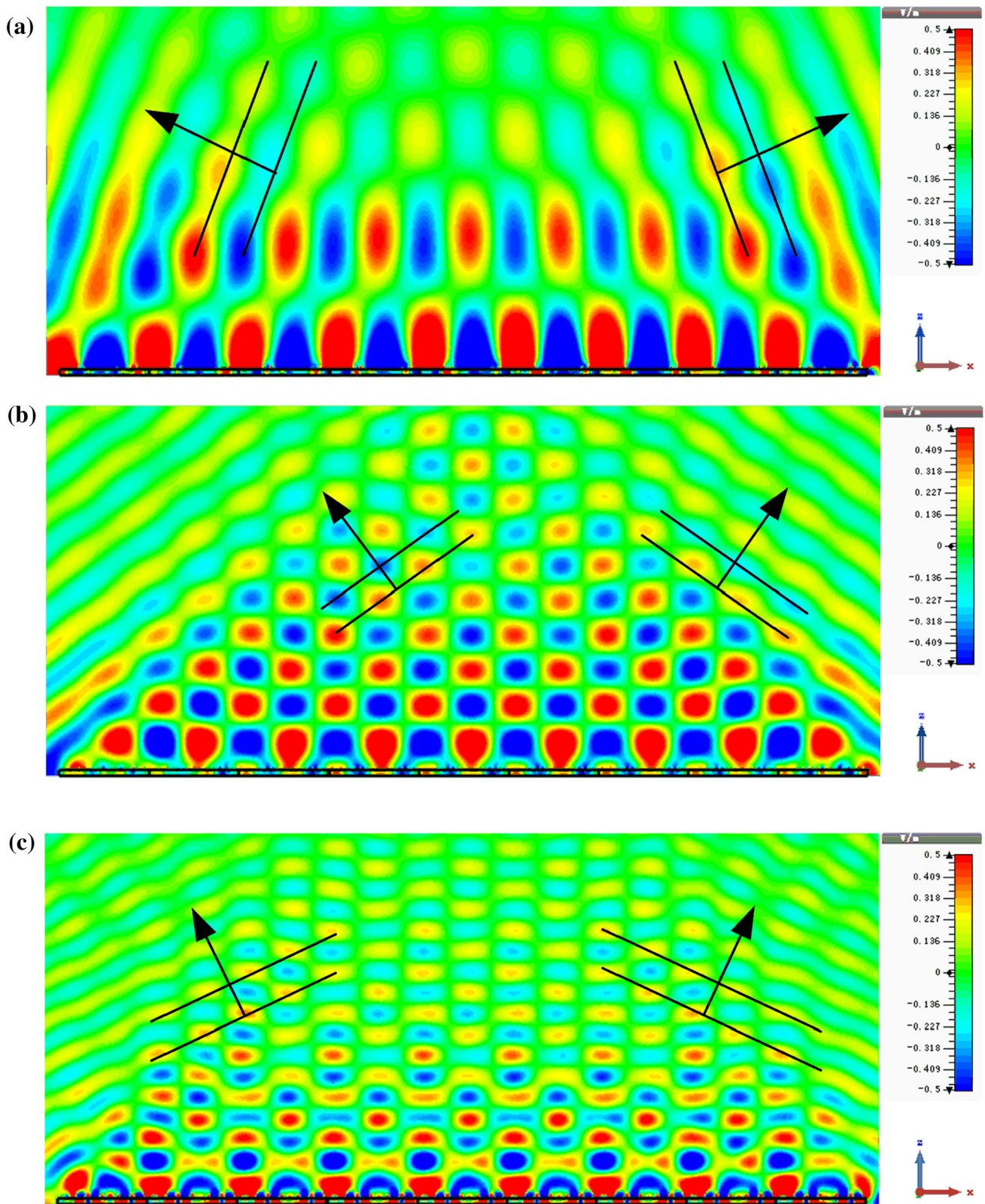


Fig. 8 Electric field distribution under LP waves incident at different frequency. **a** The electric field distribution at 8.63 GHz, $\theta_r = 61^\circ$ **b** The electric field distribution at 12.23 GHz, $\theta_r = 38^\circ$ **c** The electric field distribution at 18.07 GHz, $\theta_r = 24.7^\circ$

To further elaborate the mechanics of the PB phase based PGMs, we used CST to simulate the phase shift of unit cell with different rotation angle. As can be seen in Fig. 6, the amplitude and phase were given, and it's obviously that where there exists a rotation angle $\alpha = 30^\circ$, there exists approximately $\Delta\varphi = \pi/3$ phase shift. And during the working bandwidth, the reflection amplitude remains in a high efficiency for 97%.

To achieve high efficient anomalous reflection, we construct the PGM formed by six unit cells with different rotation angle shown in Fig. 6b. The co-polarization reflection unit cell rotates from 0 to $5\pi/6$ with $\pi/6$ step width Fig. 7 shows the phase and amplitude of six unit cells. What's more, CST numerical simulation was performed to demonstrate its anomalous reflection properties. We use field monitor to track distribution of the electric field under LP waves incidence and the results were shown in Fig. 8. From the figure, it is clearly shown that the perpendicular incident waves did not reflect perpendicularly back, but reflected at θ_r . And the reflective angle decreased as the frequency grew. It showed that the reflective angle $\theta_r = 61^\circ, 38^\circ, 24.7^\circ$, when the incident wave frequency $f = 8.63, 12.23,$

18.07 GHz, respectively. All the results were in good accordance with anomalous reflection formulation.

5 Experiment and result analysis

To further verify our previous theoretic analysis and simulation, $237.6 \text{ mm} \times 198 \text{ mm} \times 3 \text{ mm}$ sample was fabricated by traditional PCB technology. The measured sample was displayed in Fig. 9a. We chose 3 mm thickness F4B substrate as the dielectric layer, and the surface metal pattern was copper coating. In addition, pattern were tinned to protect the structure from being oxidized. Because the circular polarization waves can be seen as a combination of a x -polarization wave and a y -polarization wave, we can use two linear polarization antennas to take place of the circular polarization antenna. As is displayed in Fig. 9b, it's the schematic of anomalous reflected measurement setup. In the experiment, we use horn antennas to provide EM waves, the measure results can be more accurate if using the focused beam. The horn antenna was used to transmit or receive x -polarization wave and a y -polarization wave by placing it on its short side or long side,

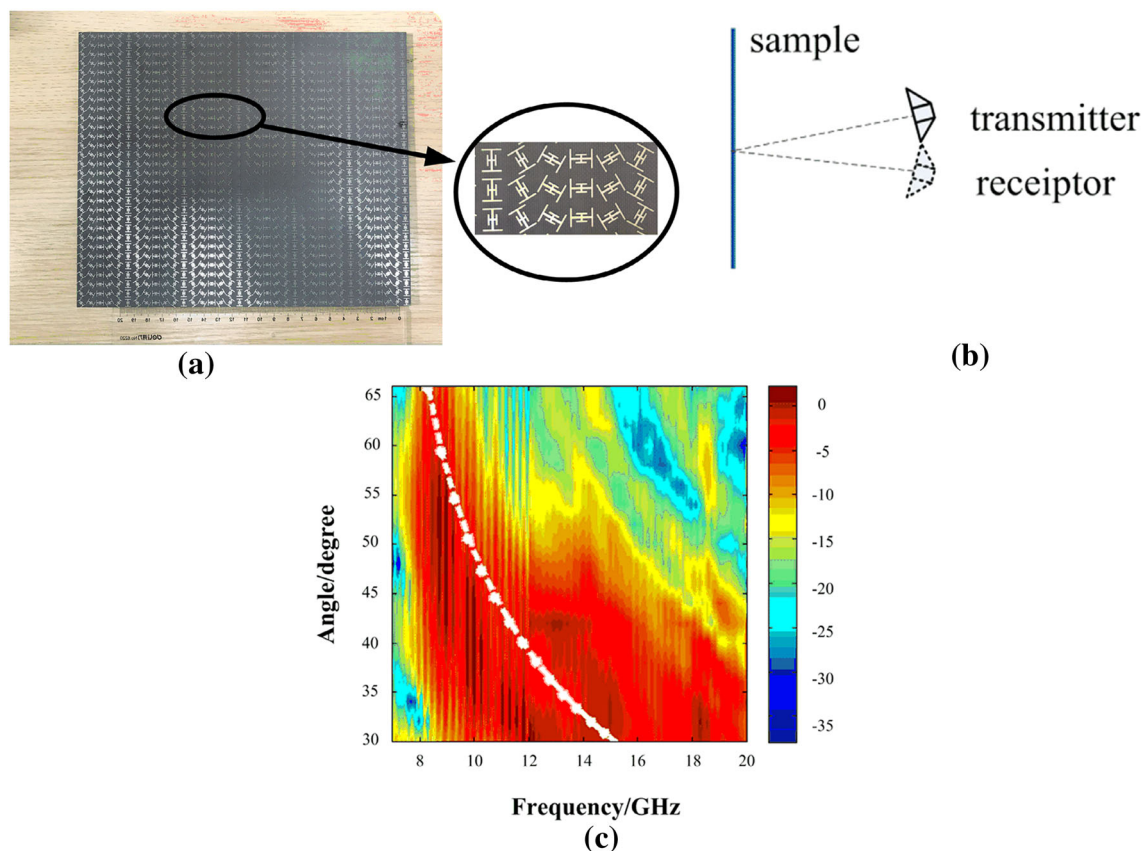


Fig. 9 **a** The schematic of sample. **b** The schematic of anomalous reflection measurement setup. **c** The results of anomalous reflection while the white curve represents the simulation results

respectively. So one of the two horn antennas served as transmitter and the other served as receiver. Because the large size of our sample ($237.6 \text{ mm} \times 198 \text{ mm} \times 3 \text{ mm}$), the diffraction effects can be neglected. Besides, the entire measurement was carried out in the anechoic chamber, and some diffractions were absorbed by the absorber. To keep two antennas are on the same height, the revolving stage is used to fix antennas, while the sample was fixed on the central vertically. First, the two revolving arms were about 4° angle between each other, and the same size metal sheet was measured as the reflective surface to normalize. Then we can measure the amplitude and phase of co- and cross-polarization of this PGM. In the measurement, we rotated the receiver antenna arm from 30° to 66° with 2° step width and obtained the r_{xy} , r_{xx} , r_{yx} , r_{yy} , φ_{xy} , φ_{xx} , φ_{yx} , φ_{yy} in working frequency band ranging from 7 to 20 GHz. Using those data, we can calculate the co- and cross-polarized reflected amplitudes and phase with different incidence angles (Fig. 9c). Above all, the measured results show a good accordance with the simulated one.

6 Conclusion

In this paper, we designed a kind of co-polarization anomalous reflection PGM with two crossed H-shaped electric dipole resonator based on PB phase. This reflective PGM can achieve ultra-broadband and high efficiency co-polarization reflection whether the incident wave is LCP or RCP. And the polarization-keeping is owing to abrupt phase change simultaneously in both x -direction and a y -direction, while the anomalous reflection is produced by phase gradient based on PB phase. The simulation indicates that the co-polarization reflection efficiency was more than 97% during the working spectrum ranging from 8.17 to 19.3 GHz. It is worth mentioning that the high efficiency anomalous reflection may have many applications, such as RCS reduction and stealthy technology.

Acknowledgements The authors are grateful to the support from the National Natural Science Foundation of China (Grants No. 61501497, 615601507).

References

1. C. Pfeiffer, A. Grbic, *Phys Rev Lett* **110**(19), 197401 (2013)
2. S. Sun, K.Y. Yang, C.M. Wang et al., *Nano Lett* **12**(12), 6223–6229 (2012)
3. J. Wang, S. Qu, H. Ma et al., *Appl Phys Lett* **101**(20), 201104 (2012)
4. N.K. Grady, J.E. Heyes, D.R. Chowdhury et al., *Science* **340**(6138), 1304–1307 (2013)
5. N. Yu, P. Genevet, M.A. Kats et al., *Science* **334**(6054), 333–337 (2011)
6. Y.Y. Sun, L. Han, X.Y. Shi, Z.N. Wang, D.H. Liu, *Acta Phys Sin* **62**, 104201 (2013). (in Chinese)
7. D. Wang, J. Zhang, J. Yu, *J Air Force Eng Univ* **17**(3), 85–88 (2016). (in Chinese)
8. Y.F. Li, J.Q. Zhang, S.B. Qu et al., *Acta Phys* **63**, 084103 (2014). (in Chinese)
9. D. Lin, P. Fan, E. Hasman et al., *Science* **345**(6194), 298 (2016)
10. Y. Yang, W. Wang, P. Moitra et al., *Nano Lett* **14**(3), 1394 (2014)
11. Y.F. Yu, A.Y. Zhu, R. Paniagua-Domínguez et al., *Laser Photonics Rev* **9**(4), 412–418 (2015)
12. S. Kruk, B. Hopkins, I.I. Kravchenko et al., *Apl Photonics* **1**(3), 917 (2016)
13. M.J. Lockyear, A.P. Hibbins, J.R. Sambles, *Phys Rev Lett* **102**, 073901 (2009)
14. A.P. Hibbins, J.R. Sambles, C.R. Lawrence, *J Appl Phys* **86**, 1791 (1999)
15. A.P. Hibbins, J.R. Sambles, C.R. Lawrence, *Phys Rev E* **61**, 5900 (2000)
16. H.L. Zhu, S.W. Cheung, K.L. Chung et al., *IEEE Trans Antenn Propag* **61**, 4615 (2013)
17. Y. Li, J. Zhang, S. Qu et al., *J Phys D Appl Phys* **47**(42), 425103 (2014)
18. S.L. Sun, Q. He, S.Y. Xiao, Q. Xu, X. Li, L. Zhou, *Nat Mater* **11**, 426 (2012)
19. L. Huang, X. Chen, H. Mühlenbernd et al., *Nano Lett* **12**(11), 5750–5755 (2012)
20. L. Yong-Feng, Z. Jie-Qiu, Q. Shao-Bo et al., *Chin Phys B* **24**(1), 014202 (2015)
21. Y. Zhao, A. Alù, *Phys Rev B* **84**(20), 205428 (2011)
22. J.K. Gansel, M. Thiel, M.S. Rill et al., *Science* **325**(5947), 1513–1515 (2009)
23. Y.J. Chiang, T.J. Yen, *Appl Phys Lett* **102**(1), 011129 (2013)
24. Y. Li, J. Zhang, S. Qu et al., *J Appl Phys* **115**(23), 234506 (2014)
25. L. Fassarella, *Revista Brasileira De Ensino De Física* **29**(2), 215–224 (2007)